HHS Public Access

Author manuscript

J Am Chem Soc. Author manuscript; available in PMC 2016 June 17.

Published in final edited form as:

J Am Chem Soc. 2015 June 17; 137(23): 7404–7414. doi:10.1021/jacs.5b03042.

A Fluorogenic Aryl Fluorosulfate for Intraorganellar Transthyretin Imaging in Living Cells and in *Caenorhabditis elegans*

Aleksandra Baranczak[1,2], **Yu Liu**[1,2], **Stephen Connelly**[2], **Wen-Ge Han Du**[3], **Erin R. Greiner**[1,2], **Joseph C. Genereux**[1,2], **R. Luke Wiseman**[2,4], **Yvonne S. Eisele**[1,2], **Nadine C. Bradbury**[3], **Jiajia Dong**[1], **Louis Noodleman**[3], **K. Barry Sharpless**[1,6], **Ian A. Wilson**[3,6], **Sandra E. Encalada**[2,5,7,*], and **Jeffery W. Kelly**[1,2,6,*]

[1]Department of Chemistry, The Scripps Research Institute, 10550 North Torrey Pines Road, La Jolla, USA

[2]Department of Molecular and Experimental Medicine, The Scripps Research Institute, 10550 North Torrey Pines Road, La Jolla, USA

[3]Department of Integrative Structural and Computational Biology, The Scripps Research Institute, 10550 North Torrey Pines Road, La Jolla, USA

[4]Department of Chemical Physiology, The Scripps Research Institute, 10550 North Torrey Pines Road, La Jolla, USA

[5]Department of Molecular and Cellular Neuroscience, The Scripps Research Institute, 10550 North Torrey Pines Road, La Jolla, USA

[6]The Skaggs Institute for Chemical Biology, The Scripps Research Institute, 10550 North Torrey Pines Road, La Jolla, USA

[7]Dorris Neuroscience Center, The Scripps Research Institute, 10550 North Torrey Pines Road, La Jolla, USA

Abstract

Fluorogenic probes, due to their often greater spatial and temporal sensitivity in comparison to permanently fluorescent small molecules, represent powerful tools to study protein localization and function in the context of living systems. Herein, we report fluorogenic probe **4**, a 1,3,4-oxadiazole designed to bind selectively to transthyretin (TTR). Probe **4** comprises a fluorosulfate group not previously used in an environment-sensitive fluorophore. The fluorosulfate functional group does not react covalently with TTR on the timescale required for cellular imaging, but does red shift the emission maximum of probe **4** in comparison to its non-fluorosulfated analog. We demonstrate that probe **4** is dark in aqueous buffers, whereas the TTR•**4** complex exhibits a fluorescence emission maximum at 481 nm. The addition of probe **4** to living HEK293T cells

[*]corresponding authors: jkelly@scripps.edu, encalada@scripps.edu.
Current address for Stephen Connelly is aTyr Pharma, 3545 John Hopkins Court, Suite 250, San Diego, CA 92121

Supporting Information. Supplementary Tables, Figures, Experimental Details and Synthetic Methods are supplied as Supporting Information. This material is available free of charge via the Internet at http://pubs.acs.org.

allows efficient binding to and imaging of exogenous TTR within intracellular organelles, including the mitochondria and the endoplasmic reticulum. Furthermore, live *Caenorhabditis elegans* expressing human TTR transgenically and treated with probe **4** display TTR•**4** fluorescence in macrophage-like coelomocytes. An analog of fluorosulfate probe **4** does react selectively with TTR without labeling the remainder of the cellular proteome. Studies on this analog suggest that certain aryl fluorosulfates, due to their cell and organelle permeability and activatable reactivity, could be considered for the development of protein-selective covalent probes.

INTRODUCTION

While temporal and spatial localization of a protein-of-interest (POI) has historically been accomplished by fusing the POI to a fluorescent protein or small-molecule-regulated fluorescent protein tag[1–9], there is growing interest in the development of fluorogenic small molecule probes that directly target proteins-of-interest (PsOI). Fluorogenic probes are defined as fluorophores exhibiting a fluorescent signal only upon binding to or binding to and reacting with the POI in the context of a complex biological environment[10–17]. While notable success with fluorogenic probes has been realized, several challenges remain. For example, the majority of fluorogenic probes published to date target enzymes[4,7,14,18–24]. It would be ideal if fluorogenic probes could be routinely developed for non-enzyme proteins and other macromolecules[8,13,15,16,25–30]. Moreover, a better understanding of the physicochemical underpinnings of fluorogenicity would enable more efficient design[18,31,32]. Numerous applications are expected to result from the development of fluorogenic small molecule probes for important PsOI. For example, probes exhibiting good cell permeability, POI binding selectivity, fast labeling kinetics (assuming covalent probes are sought), and desirable excitation and emission wavelengths can be applied in the design of pulse-chase experiments within cells to follow POI trafficking and degradation kinetics.

Several different mechanisms contribute to fluorogenicity in small molecules[18,32]. One origin requires an environment-sensitive (solvatochromic) chromophore, whose fluorescent properties (excitation and emission wavelengths, quantum yields, etc.) depend both on the structure of the chromophore and on the microenvironment of the protein binding site. Environment-sensitive fluorophores are generally dark in aqueous solution, but fluoresce when the chromophore is placed in a hydrophobic membrane environment or in a hydrophobic protein binding site[10,33–35].

We are interested in developing solvatochromic fluorogenic probes to study the protein transthyretin. Transthyretin (TTR) is a non-enzyme protein synthesized by the liver for secretion into the blood and produced by the choroid plexus for secretion into the cerebrospinal fluid[36]. TTR serves as a transporter of holo-retinol-binding protein and/or thyroxine depending on its localization[36,37]. TTR is composed of 127-amino-acid, β-sheet-rich subunits that associate into a tetramer (Figure 1). Tetramer dissociation is rate limiting for TTR aggregation, which drives the pathology of several degenerative diseases[38]. The dimer-dimer interface bisected by the C_2 or Y axis creates the two funnel-shaped thyroxine

(T_4)-binding sites that are >99% unoccupied, except in tissues bathed by the cerebrospinal fluid[39] (Figure 1A and B).

We have used fluorogenic TTR probes to understand how the cellular proteostasis network affects TTR folding efficiency[17], and to quantify the kinetic stabilization (measured by the rate of TTR dissociation) afforded by oral tafamidis or diflunisal treatment (drugs that prevent amyloidogenesis)[40–44]. Encouraged by the development of TTR-selective fluorogenic probes for the aforementioned uses, as well as for additional applications[15,16,25,35], we explored the design of additional environment-sensitive, cell-permeable fluorogenic TTR probes wherein the little studied aryl fluorosulfate group ($ArOSO_2F$) is incorporated[45].

Previously, we reported the fluorogenic 1,3,4-oxadiazole-based sulfonyl fluoride **1** (Figure 2A), that upon binding and subsequent reaction with the pK_a-perturbed Lys-15 ε-amino group within the two thyroxine binding sites of the TTR tetramer creates a fluorescent conjugate[25]. The goal of this study was to evaluate the applicability of 1,3,4-oxadiazole-based aryl fluorosulfates as fluorogenic TTR probes. 1,3,4-oxadiazole-based aryl fluorosulfates were employed to assess the localization of natively folded tetrameric TTR within transgenic *C. elegans*, and to assess their potential to react with TTR[15,16,25], as well as to examine their general proteome reactivity in cells. Herein, we report on a *para*-sulfonyl fluoride **2** not studied previously, as well as structurally analogous aryl fluorosulfate candidate probes **3** and **4** (Figure 2A). Candidate probe **4** is an environment-sensitive fluorophore that selectively binds to TTR and renders the TTR•**4** complex fluorescent in subcellular compartments of living cells and within coelomocytes of living worms. Unlike probes **1**–**3**, probe **4** does not react covalently with TTR significantly on the time scale of the imaging experiments.

EXPERIMENTAL SECTION

Crystallization and structure determination of TTR^{WT} complexes

TTR^{WT} was concentrated to 6.94 mg/mL in 10 mM sodium phosphate buffer (pH 7.6) with 100 mM KCl and cocrystallized at room temperature with a 5 molar excess of each candidate ligand (2.5 molecules per T_4-binding site) using the vapor-diffusion sitting drop method. All crystals were grown from 1.395 M sodium citrate, 3.5% v/v glycerol at pH 5.5 as the mother liquor and appeared after one week. The crystals were cryo-protected with mother liquor containing 10% v/v glycerol.

Data were collected at beam-line 11-1 at the Stanford Synchrotron Radiation Lightsource (SSRL) at a wavelength of 0.9795 Å. All diffraction data were indexed, integrated, and scaled using HKL2000 in orthorhombic space group $P2_12_12$ with two promoters per asymmetric unit (half a tetramer)[46]. Model building and refinement was carried out using Coot and Refmac5[47,48]. Ligand coordinate and restraint files were generated using JLigand and ligands were assigned an occupancy of 0.5 to account for the ligand residing on the C_2 axis[49]. Hydrogens were added during refinement, and anisotropic *B*-values were calculated. Final models were validated using the JCSG quality control server v2.8 (http://smb.slac.stanford.edu/jcsg/QC/) incorporating MolProbity, ADIT (http://rcsb-

deposit.rutgers.edu/validate) WHATIF, and Resolve[50–52]. Data collection and refinement statistics are summarized in Table S2.

Confocal fluorescence microscopy detection of TTR in cultured live cells

For Figure 5, HEK293T cells were plated on chambered coverglasses (Thermo-Fischer) ~20 h after transfection. After 24 h, fresh DMEM (FBS-free) containing MitoTracker® Orange CMTMRos (Life Technologies, 500 nM) and NucRed® Live 647 Ready Probes® Reagent (Life Technologies, solution prepared according to manufacturer's recommendations) and probe **4** (20 μM) was added and the cells were incubated at 37 °C under 5% CO_2. After 20 min, fresh DMEM (FBS-free) was added. After 30 min incubation at 37 °C, DMEM was replaced with DPBS and the cells were imaged using a Zeiss LSM 710 laser scanning confocal microscope (LSCM) attached to a Zeiss Observer Z1 microscope equipped with the infinity corrected optics: 63x oil Plan Apo, 1.4na DIC. The following lasers were used for imaging: 405 nm excitation for detection of probe **4**, 561 nm excitation for detection of MitoTracker® Orange, and 633 nm excitation for detection of NucRed®. Appropriate holistic prism based emission was used to detect the signal of each of the dyes respectively. For Figures 6 and 7, HEK293T cells were plated in chambered coverglasses (Thermo-Fischer) ~20 h after transfection. After 24 h, fresh DMEM (FBS-free) containing MitoTracker® Orange (500 nM) and NucRed® (solution prepared according to manufacturer's recommendations) was added and the cells were incubated at 37 °C under 5% CO_2. After 20 min, DMEM was replaced with DPBS containing probe **4** (5 μM). After ~30 sec, fresh solution of DMEM (FBS-free) was added. After 10–15 min, DMEM was replaced with DPBS and the cells were imaged as above.

C. elegans methods and strains

N2 Bristol was used as the wild-type strain; standard nematode culture methods and genetics were followed as described previously[53]. Nematodes were grown on NGM plates seeded with the *E. coli* strain OP50 at 20 °C. The following transgenic strains were used: CL2008 *him-5(e1490) V; dvIs3[unc-54p::hTTR(WT) + rol-6]* was provided by C. Link (University of Colorado). The strain CX11480 *kyEx3017[des-2p::myr::gfp + unc-122p::DsRed]* was provided by C. Bargmann (Rockefeller University). Integration of *kyEx3017* was done by gamma irradiation following standard methods[54]. Integrated strains were backcrossed at least four times into an N2 wild-type background. The strain LG398 *geIs101[rol-6(su1006)]* was ordered from the *Caenorhabditis* Genetics Center (CGC). The following strains were made for live-imaging with probe **4**: SEE055 *geIs101[rol-6(su1006)]; kyEx3017[des-2p::myr::gfp + unc-122p::DsRed]* and SEE084 *him-5(e1490) V; dvIs3[unc-54p::hTTR(WT) + rol-6]; scrIs010[des-2p::myr::gfp + unc-122p::DsRed]*.

In vivo C. elegans imaging

Ten L4 larvae of each of the two strains SEE055 *geIs101[rol-6(su1006)]; kyEx3017[des-2p::myr::gfp + unc-122p::DsRed]* and SEE084 *him-5(e1490) V; dvIs3[unc-54p::hTTR(WT) + rol-6];scrIs010[des-2p::myr::gfp + unc-122p::DsRed]* were transferred into a 96-well plate containing 150 μL liquid culture media (S-complete media with 50 μg/mL carbenicillin, 0.1 μg/mL amphotericin B, 5 mg/mL OP50, 120 nM

fluorodeoxyuridine)[55]. Worms were mixed on a nutator and incubated overnight at 20 °C. On day 1 of adulthood, probe **4** (0.5 μL of a 3 mM solution in DMSO) was added to the worm solution (final concentration 10 μM). Worms were mixed well on a nutator and incubated overnight at 20 °C. On day 2 of adulthood, worms were collected and washed three times in 1 mL M9 buffer and transferred to a fresh 6 cm NGM plate prior to image analysis.

For light and fluorescence microscopy, animals were mounted in 2% sodium azide buffer (prepared in 1x PBS) on 3% agarose pads and covered with a coverslip. Imaging of coelomocytes was done on live animals with simultaneous differential interference contrast microscopy (DIC) and epifluorescence modalities using a Nikon Ti-E Perfect Focus inverted microscope equipped with a iXon+ DU897 EM Camera, either a 40X oil or a 100X/1.49 NA oil objective and an Intensilight System M lamp and 340–380 nm/500–550 nm excitation and emission filters, respectively, to detect probe **4** fluorescence, and 545–570 nm/578–625 nm emission and excitation filters, respectively, to detect DsRed fluorescence.

RESULTS

Reported for the first time in the 1930's[56], aryl fluorosulfates (the functional group in probes **3** and **4**; recently studied more comprehensively[45]) have been reported in less than 20 publications and patents. The paucity of publications is likely due to the inconvenient synthetic methodology of the past[57,58], as well as the perception that aryl fluorosulfates would be highly reactive and, therefore, incompatible with biological applications. However, as recently demonstrated by the Sharpless laboratory, the reactivity of the aryl fluorosulfate functional group is very low and vastly different from its chlorosulfate counterpart ($ArOSO_2Cl$)[45,58–60]. Aryl fluorosulfates can now easily be prepared from phenols via a reaction with the gas SO_2F_2 (sulfuryl fluoride) under basic conditions (Et_3N) in dichloromethane[45,61–63]. The resulting aryl fluorosulfates are typically produced in high yields and are remarkably stable, even at extremes of pH and temperature[45]. Moreover, aryl fluorosulfates are more stable towards acid-base catalyzed disruption at their S-(VI)-center than their deoxy relatives, i.e., aryl sulfonyl fluorides ($ArSO_2F$)[45].

Consistent with the low reactivity of aryl fluorosulfates, the synthesis of candidate aryl fluorosulfate probe **4** commenced with the installation of the fluorosulfate functional group (95% yield) onto the structure of 4-hydroxybenzoic acid (**5**), employing SO_2F_2 (sulfuryl fluoride) and Et_3N in CH_2Cl_2/H_2O (3:2)[45,63] (Figure 2B; and Supporting Experimental Methods). Subsequent acid chloride formation, coupling with hydrazide (**7**), and TsCl-mediated oxadiazole ring formation led to **8**. Demethylation in presence of L-methionine in methanesulfonic acid then generated the desired aryl fluorosulfate probe **4** in 48% overall yield[25]. The same sequence of steps was used to prepare the *meta* analog, candidate probe **3**.

We first evaluated the ability of aryl sulfonyl fluoride **2**, as well as aryl fluorosulfate probes **3** and **4**, to bind to and/or bind to and react with wild-type TTR (TTR^{WT}). Sulfonyl fluoride **1** served as a positive control for the covalent modification of TTR[25]. Probes **1**–**4** (7.2 μM) were individually incubated with recombinant TTR^{WT} (3.6 μM) for 24 h (37 °C). The possibility of conjugate formation was monitored by liquid chromatography–mass

spectrometry (LC-ESI-MS). The 2:1 ratio of small molecule to TTR^{WT} was employed because each C_2-symmetric tetramer has two small molecule binding sites (Figure 1A). Probe **4** reacted only very slowly with TTR^{WT}. There was no detectable reaction after 1 h, which is the longest unicellular imaging period utilized in this manuscript (Figure S1 and S2). A 24 h incubation period was required to observe a 6% modification yield, equal to the incubation period used for *C. elegans* imaging in this manuscript. As only 2/4 subunits of TTR are modifiable, the theoretical maximal yield of modification is 50%[64].

Surprisingly, the product detected by mass spectrometry was TTR^{WT} covalently linked to a SO_3^- functional group (mass of intact TTR^{WT} monomer = 13,892 Da, modified TTR^{WT} monomer = 13,972 Da) (Figures 2C, S1, S2, Table S1). Formation of the TTR-$(CH_2)_4$N(H)-SO_2-OAr conjugate derived from probe **4** (Figure 2C) was not detected; however, its transient presence was inferred as a reactive intermediate hydrolyzed to afford TTR-SO_3^-. We hypothesize that the hydrolysis of TTR-$(CH_2)_4$N(H)-SO_2-OAr (Figure 2C) is somehow catalyzed by TTR^{WT}, as we have not observed the hydrolysis of analogous conjugates[15,25]. The yield of TTR-SO_3^- resulting from treatment of TTR^{WT} by the *meta* probe **3** was higher, but still incomplete: 29% of TTR-SO_3^- was formed after a 24 h incubation period (Figure S2, Table S1). Notably, the simultaneous presence of the TTR-$(CH_2)_4$N(H)-SO_2-OAr conjugate derived from probe **3** (detected mass = 14,277 Da) and the hydrolysis product TTR-$(CH_2)_4$N(H)-SO_3- was detected after 1, 2 and 4 h of incubation (Figures S1 and S2, Table S1), supporting the presence of the inferred intermediate during the slow reaction between TTR and probe **4**. Further LC-MS-MS analysis of the reaction product formed from probe **3** reacting with TTR^{WT} revealed modification of the Lys-15 residue (Figure S3)[15,16,25]. No modification of the TTR^{K15A} mutant tetramer was observed when the pK_a-perturbed Lys-15 was replaced by Ala (Figure S4). The *meta* (**1**) and *para* (**2**) sulfonyl fluorides (Figure 2A), whose reaction with TTR^{WT} led to the formation of stable TTR-ligand conjugates (Figures S1, S2, Table S1), exhibited an enhanced but analogous difference in reactivity towards TTR^{WT}. The *meta* sulfonyl fluoride **1** nearly quantitatively modified TTR^{WT} after 1 h of incubation (mass of labeled TTR^{WT} monomer = 14,262 Da), as reported previously[25]. In contrast, complete modification of TTR^{WT} by the *para* sulfonyl fluoride **2** was not achieved, even after a 24 h incubation period.

To garner insight into the difference in reactivity of the *meta* and *para* aryl fluorosulfate isomers **3** and **4** with TTR^{WT}, crystal structures of the complexes and/or conjugation products were determined (1.25 Å and 1.35 Å resolution, respectively, see Table S2 for data collection and refinement statistics). Since the two-fold symmetry axis (C_2) runs through the T_4-binding site of TTR (Y-axis; Figure 1A), the resulting electron density maps of ligands within the T_4-binding sites represent an average of the opposing ligand orientations generated by the crystallographic two-fold symmetry axis, which can often hamper the modeling of non-symmetrical ligands[39].

The *F*o - *F*c electron density omit maps of the products of the reaction between probe **3** and TTR^{WT} allowed for clear placement of both the bis-phenol **9** (Figures S5 and S6) and the sulfamated Lys-15 residue comprising modified TTR^{WT} (Figure 3A) resulting from hydrolysis of the initial reaction product shown in Figure 2C. The 3,5-dichloro-4-hydroxy aryl ring was found to occupy the inner binding sub-site. The 3,5-dichloro substituents were

placed into halogen binding pocket (HBP) 3/3′, while the 4-hydroxy group formed a hydrogen bond with the Ser117/117′ side chains at the base of the T_4-binding-pocket (Figure 3A).

The *F*o - *F*c electron density omit maps of unreacted probe **4** bound to TTR^{WT} revealed probe **4** could bind in both the 'forward' and 'reverse' binding orientations within the T_4-binding pockets (Figures 3B, 3C and S7). While the overlapping core of probe **4** could be modeled into the observed *F*o - *F*c density, it was more difficult to model the flexible fluorosulfate group in the outer binding sub-site, especially at low occupancy. In the forward binding orientation, the fluorosulfate group penetrated past the S117/117′ residues into a cavity formed at the center of the TTR tetramer (Figure 3B). Since only one fluorosulfate group could physically occupy that cavity at a time, it appeared that one molecule of probe **4** bound to binding site 1 in the forward mode while the other probe **4** bound to binding site 2 in the reverse mode within the same tetramer (Figure S8). Thus, the 3,5-dichloro-4-hydroxy ring can occupy the outer binding sub-site (Figure 3B) or the inner binding sub-site (Figure 3C). Finally, the product of the very slow two-step reaction between probe **4** and TTR^{WT} (Figure 2C)—the bis-phenol **10** resulting from hydrolysis—was observed to bind in the 'reverse' orientation to sulfamated TTR based on the *F*o - *F*c electron density omit map (Figure 3D). Consequently, the 3,5-dichloro substituents were found to occupy the outer binding sub-site HBP1/1′, while the *para* phenol group was oriented into the inner T_4-binding pocket where it formed hydrogen bonds with S117/117′ (Figure 3D). Thus, we conclude that bis-phenol **10** must have dissociated and then rebound in the opposite orientation post-hydrolysis.

We next examined the photophysical properties of the sulfonyl fluoride-based probes **1** and **2**[25], and aryl fluorosulfate-based probes **3** and **4** in the absence of TTR. First, excitation and emission spectra and the values of the extinction coefficients for probes **1**, **2**, **3** and **4** were determined in dichloromethane (Table S3, Figure S9A). While all probes were found to exhibit $\lambda_{ex\ max}$ close to 300 nm, the value of $\lambda_{em\ max}$ ranged from 364 nm for probe **4** to 401 nm for its sulfonyl fluoride analog probe **2**. Generally, sulfonyl fluorides were found to be characterized by lower extinction coefficients than their fluorosulfate counterparts. Probe **4** exhibited the extinction coefficient value of 25,000 [M^{-1} cm^{-1}] (Table S3). Next, the environment sensitivity of probes **2**, **3** and **4** was tested. Importantly for the intended fluorogenic applications, the fluorescence signal of probes **2**, **3** and **4** in aqueous solution could not be detected (Figure 4, also see Figure S9B and Table S4 for a comparison of the effect of solvent polarity on fluorescence intensity, and excitation and emission wavelengths of probe **4**). Incubation of probes **1**, **2**, and **3** (7.2 μM) with recombinant TTR^{WT} (3.6 μM) for 1 h led to the formation of fluorescent conjugates in the cases of probes **1** and **2** (Figure 4 and Figures S2, S10, Table S5) or mostly a non-covalent fluorescent complex with probe **3** (Figures 4 and S2). Incubation of probe **4** (7.2 μM; $\lambda_{ex\ max}$ = 345 nm, $\lambda_{em\ max}$ = 481, Table S5) with TTR led to the formation of a fluorescent non-covalent complex (Figure 4), as demonstrated by a time dependent LC-ESI-MS analysis (Figure S1, S2, Table S1). Notably, the fluorescence intensity of the non-covalent complex between TTR^{WT} and probe **4** (TTR•**4**; after 1 h of incubation) was five times higher than the fluorescence intensity of the previously reported TTR-sulfonyl fluoride **1** conjugate, and about twenty times higher than

the emission from the TTR-sulfonyl fluoride **2** conjugate (Figure 4). The TTR•**4** complex exhibited a higher fluorescence intensity than the analogous TTR•**3** complex (small amount of conjugate formation; Figure 4; $\lambda_{ex\ max}$ = 338 nm, $\lambda_{em\ max}$ = 488 nm for TTR•**3** complex, Table S5).

Interestingly, extended incubation of probe **3** with recombinant TTR^{WT} led to noticeable changes in the fluorescence emission spectra, likely because of the Lys15–εNH-SO_3^- sulfamate contribution (29% sulfamation after 24 h of incubation) and the linked contribution from binding of the bis-phenol **9** (Figure 3A, S11A, S11B, Table S5). In contrast, the TTR•**4** non-covalent complex dominated the fluorescence spectrum, even after 24 h (Figure S11C, S11D, Table S5), despite ≤ 6% sulfamation (Figure S2), indicating that the solvatochromic fluorescence enhancement is more significant than the reactivity-based turn-on, unlike the situation with sulfonyl fluorides[25].

We next assessed the applicability of probe **4** for TTR imaging in living cells by examining the ability of probe **4** to bind to TTR tetramers localized to different subcellular compartments, including mitochondria. It is very challenging to deliver non-lipophilic cation probes or drug-like molecules into mitochondria, as reflected by the limited number of non-lipophilic cation small molecules that successfully target this organelle, despite its connection to a variety of diseases[65,66]. The established paradigm for creating mitoactive small molecule probes requires the attachment of a large, lipophilic cation to a substructure targeting a mitochondrial protein-of-interest, which results in the accumulation of these small molecules inside mitochondria as a consequence of the mitochondrion's large, negative electrochemical cross-membrane potential[67,68]. Probe **4** lacks this consensus feature. To evaluate the capacity of probe **4** to image TTR targeted to mitochondria, we prepared TTRs targeted to mitochondria by a COXVIII mitochondrial targeting sequence, similar to the approach previously described for a monomeric TTR variant (^{mt}M-TTR^{WT})[69]. For these experiments, we used the destabilized TTR variants L55P and V30M, since these variants are more efficiently imported and retained in mitochondria. This was shown by the processing of the N-terminal targeting sequence, as analyzed by immunoblot analysis (Figures S12A and S13A). In contrast, the more stable wild-type $^{mt}TTR^{WT}$ accumulated both in the cytosol and mitochondria (Figures S12A and B), presumably due to its stable tetramerization interfering with mitochondrial import. As shown in Figure S14, probe **4** created equivalently bright fluorescent complexes with tetrameric recombinant TTR^{V30M} and TTR^{WT} *in vitro*, whereas the fluorescence intensity of the TTR^{L55P}•**4** tetramer was slightly lower in buffer, indicating that probe **4** should be efficient at detecting intracellular levels of these mutants.

The subcellular localization of $^{mt}TTR^{L55P}$ and $^{mt}TTR^{V30M}$ in HEK293T cells was analyzed using confocal microscopy. Transfected cells were incubated with media containing probe **4** (20 μM) for 20 min at 37 °C. Simultaneous treatment with MitoTracker® Orange and NucRed® in the same media allowed parallel visualization of mitochondria and nuclei, respectively (Figure 5). The media was removed and the cells were incubated for 30 min in probe-free media. In cells expressing $^{mt}TTR^{L55P}$ or $^{mt}TTR^{V30M}$ treated with probe **4**, fluorescence from the TTR•**4** complex colocalized with a mitochondrial marker (Figure 5). No fluorescence was observed in empty vector (EV)-transfected control cells treated with

probe **4**. The images in Figure 5 constitute the first evidence for the ability of probe **4** to selectively label TTR localized to the mitochondria of living cells. In contrast and for unknown reasons, probe **3** was found to colocalize to a lesser extent with mitochondria, and fluorescence was detected in what are likely non-mitochondrial subcellular compartments (Figure S15).

To further examine the selectivity of aryl fluorosulfates **3** and **4** in the context of the human cellular proteome, HEK293T cells transfected with $^{mt}TTR^{L55P}$ variant or control cells lacking variant TTR expression were incubated with probes **3** or **4** (100 μM) for 1 h or 6 h (37 °C). Native gel analysis revealed TTR binding and fluorescence in lysates of cells transfected with $^{mt}TTR^{L55P}$, comparable to recombinant TTR^{WT} pre-incubated with each probe (Figure S16A and S16B). TTR was not detected by probe **3** or probe **4** in control samples lacking TTR overexpression, indicating that these cells either lack or have very low levels of endogenous TTR passing through the secretory pathway. Even though off-target labeling could be observed for probes **3** and **4**, both aryl fluorosulfates were found to be generally unreactive towards the proteome. No noticeable changes in the degree of labeling could be observed when comparing 1 h to 6 h (Figure S16A and S16B). Importantly, the small molecule treatment period in these experiments was conducted on a time scale four to twenty times longer than the fluorescence-based cellular imaging timescale discussed below.

Next, to test the sensitivity of probe **4**, we further optimized the conditions for the detection of TTR variants in mitochondria in terms of the treatment period (Figure S17), the post-treatment probe-free incubation period (Figure S18), and the probe **4** concentration (Figure S19). Clear detection of mitochondrial TTR using probe **4** was achieved by treating live cells with a 5 μM concentration of probe **4** for 30 sec, followed by a post-treatment probe-free incubation period of 10–15 min in media. The accumulation of $^{mt}TTR^{V30M}$ and $^{mt}TTR^{L55P}$ in the mitochondria imaged by probe **4** using these conditions is clear (Figure 6). Expression of endoplasmic reticulum (ER)-targeted TTR ($^{er}TTR^{WT}$) in the secretory pathway of HEK293T cells also enabled facile imaging of TTR in the ER (Figures 7 and S13B).

Finally, to further demonstrate the applicability of probe **4** for imaging the location of TTR in a living multi-cellular organism, we treated *C. elegans* expressing human TTR^{WT} in the body wall muscle under the *unc-54p* body wall muscle promoter *(him-5; unc-54p::hTTR(WT) + rol-6*)[70] with probe **4** (10 μM). Control (*rol*-6) worms lacking TTR^{WT} expression were also treated with probe **4** (10 μM). In both the TTR transgenic and in the control worms, probe **4** was applied overnight to the medium of day 1 old adult *C. elegans* grown in liquid culture in 96-well plates.[55,71] The day 2 old adult worms pretreated with probe **4** were then placed on agarose pads and imaged using epifluorescence microscopy after *C. elegans* immobilization with sodium azide.[72] We imaged within a 24 hour period from treatment because less than 6% covalent modification of TTR by probe **4** was observed after 24h *in vitro* (Figure S2 and Table S1), an extent of reaction that does not alter the observed fluorescence emission spectra (Figure S11D). We detected probe **4** fluorescence specifically in six distinct cells that resembled coelomocytes, macrophage-like scavenger cells in the body cavity (pseudocoelom) of the worm that are highly active in

endocytosis and degradation of soluble molecules (Figure 8).[73] To test whether probe **4** localized to coelomocytes, we visualized coelomocytes in probe **4**-treated TTR^{WT} and control worms expressing a fluorescent tag under the *unc-122* promoter (UNC-122::DsRed), which is expressed in all coelomocytes.[74] The TTR•**4** complex colocalized with UNC-122::DsRed in all six coelomocytes in TTR^{WT} (n = 19/21), but not in control animals (n = 0/11; Figures 8, S20).

The amount of TTR secreted from a mammalian cell has been previously shown to be modestly increased (≈ 20%) if high concentrations of a small molecule TTR probe is incubated with the cells for a period exceeding the half-life of TTR secretion (≈ 4 h from eukaryotic cells) owing to pharmacologic chaperoning.[75] Pharmacologic chaperoning results when a small molecule binds to the TTR tetramer in the endoplasmic reticulum, shifting the folding equilibrium at the expense of endoplasmic reticulum-associated degradation. Thus, we hypothesize that pharmacologic chaperoning by probe **4** will dose-dependently and modestly increase the amount of TTR secreted by *C. elegans* during the overnight preimaging period utilized in this paper. This is not a consideration in the cell-based experiments presented above, which are completed in < 1 h.

DISCUSSION

In our quest to develop new fluorogenic probes for studying TTR, we decided to evaluate the photophysical parameters and reactivity of fluorosulfate probes[45]. This effort revealed that fluorosulfates are suitable functional groups to replace more traditional electron-withdrawing groups in solvatochromic fluorophores. For our purpose, we utilized 2,5-diphenyl-1,3,4-oxadiazole-based chromophores, which due to their photophysical properties, and thermal and chemical stability, have been widely applied in the development of optical materials, e.g., OLEDs, and fluorophores[76–79]. Many 1,3,4-oxadiazoles have been developed for applications in medicinal chemistry[80]. However, to the best of our knowledge, probes **1**–**4** and their analogs reported previously, are the only examples of fluorogenic probes targeting a specific POI[25].

In particular, probe **4** is an environment-sensitive fluorophore whose emission is very low in aqueous buffers, but is restored upon binding to TTR. In comparison to the previously reported sulfonyl fluoride probe **1**, which forms a conjugate with TTR, non-covalent binding of probe **4** to TTR exhibited blue-shifted excitation and emission maxima ($\lambda_{ex\ max}$ = 345 nm and $\lambda_{em\ max}$ = 481 nm vs $\lambda_{ex\ max}$ = 365 nm and $\lambda_{em\ max}$ = 520 nm for the TTR-**1** conjugate), and higher quantum yield upon formation of a probe **4**•TTR^{WT} complex (0.44 vs 0.19 for the TTR-**1** conjugate). We showed that probe **4** could be used as a subcellular marker to detect TTR localization in living cells (Figures 6 and 7). To the best of our knowledge, probe **4** is the first example of a fluorogenic small molecule meeting the Lipinski rule of five criteria that selectively targets a POI inside the mitochondrial matrix[81]. Due to its excellent cell permeability, time-lapse imaging (Figure S18) revealed that aryl fluorosulfate **4** undergoes very fast diffusion across various membranes before accumulating in the compartment of the cell containing TTR. First, probe **4** bound to the hydrophobic plasma membrane, as well as the ER and mitochondrial membranes, which restored the

fluorescence of probe **4** that is dark in aqueous solution. Within 15 min, probe **4** localized to the compartment harboring TTR (Figure S18).

While probe **4** was found to form a non-covalent complex with TTR^{WT} on the timescale of the imaging experiments, extended treatment of TTR^{WT} with probe **4** (24 h) led to TTR^{WT} sulfamation (6%, Table S1). Our data suggest that sulfamated TTR (TTR-$(CH_2)_4$N(H)-SO_3^-) is generated in a two-step reaction, consisting of the initial nucleophilic attack by the pK_a-perturbed Lys-15 ε-amino group on the fluorosulfate S atom, resulting in the displacement of the fluorine atom, a reaction apparently catalyzed by TTR binding and activation of the normally unreactive fluorosulfate functional group (Figure 2C)[45]. We hypothesize that fluorosulfate activation could result from hydrogen bond formation between the fluorine atom and a TTR residue within the T_4-binding pocket[82–84] or via interfacial or electric field effects[85]. Formation of the conjugate (TTR-$(CH_2)_4$N(H)-SO_2-OAr) was then followed by a relatively rapid hydrolysis step, apparently catalyzed by TTR, where the activated water molecule attacked the S atom, affording a non-covalently bound phenol and TTR sulfamated on the Lys-15 ε-amino group, i.e., TTR-$(CH_2)_4N(H)SO_3^-$ (Figure 2C).

We believe that the hydrolytic reactivity of TTR-$(CH_2)_4$-NH-SO_2-OAr is a special case. For most proteins, we hypothesize that this adduct will be resistant to hydrolysis[45], but this remains to be proven. Irreversible protein modification through functional group transfer has been reported previously, e.g., the aspirin-mediated inhibition of COX enzymes results from transfer of an acetyl group onto a serine residue[86–88]. The effect of sulfamation on TTR properties remains to be elucidated, as probes **3** and **4** were found to stabilize TTR structure and prevent fibril formation independently from the degree of covalent modification, as measured by the previously reported acid-induced fibril formation assay (Figure S21, S22)[42,89–91].

It is unclear at this juncture whether the generally lower reactivity of the fluorosulfates relative to the sulfonyl fluorides (Figure 2A) results from a non-optimal reaction geometry owing to the extra oxygen atom in the fluorosulfates, the lower inherent reactivity of fluorosulfates vs. sulfonyl fluorides (the most likely explanation), or both. Another possible contributor to the observed differences in reactivity of probes **1**–**4** may derive from distinctions in their TTR binding cooperativity. Probe binding to the two T_4-binding sites TTR, can be negatively cooperative, non-cooperative or positively cooperative[91], likely due to conformational changes within TTR. Isothermal titration calorimetry revealed that probe **4** (non-covalent binder on the time scale of the unicellular imaging experiments) bound to TTR^{WT} with negative cooperativity (K_{d1} = 2 nM and K_{d2} = 719 nM, Figure S23).

Fluorescent small molecule ligands have proven to be valuable for a variety of applications[92,93]. The next generation of fluorophores, i.e., fluorogenic probes that only exhibit fluorescence upon binding the POI in the context of a complex biological environment, are gaining in popularity as they eliminate the need for additional washout steps to reduce the high fluorescence background typically resulting from the presence of unreacted or nonspecifically bound permanently fluorescent small molecules. Additionally, application of fluorogenic protein-selective probes excludes the need to attach an inherently

fluorescent protein or small molecule-based fluorescent protein tag to the POI. Herein, we demonstrate that fluorogenic probe **4** can detect and localize eoverexpressed TTR within mammalian cells and in living *C. elegans*. Previous fluorogenic molecules have been used for detection of phosphatases in cells and in *Drosophila* brains[24], but these studies required the delivery of the fluorogenic probes into cells with cell-penetrating peptides. The advantage of probe **4** is that it can be efficiently delivered into cells and cellular organelles, without the need to append a membrane-penetrating substructure to the fluorophore. In addition, the selectivity of probe **4** to bind to the folded TTR tetramer allows the distinction of this TTR conformer over other conformations lacking a probe **4** binding site, such as misfolded TTR or TTR aggregates. The use of fluorogenic probes in living systems could provide invaluable insights into the kinetics of TTR secretion and degradation, and how these processes could be modulated therapeutically to ameliorate the TTR amyloidoses.

CONCLUSION and PERSPECTIVE

In summary, the data presented herein validate the use of the non-covalent, fluorogenic, small molecule aryl fluorosulfate probe **4** for the imaging of properly folded TTR within organelles in living cells. Moreover, probe **4** detected TTR in six macrophage-like cells in the multicellular organism *C. elegans*. Creating high affinity (K_{d1}=2 nM), selective fluorogenic probes for TTR is part of a broader effort by many researchers to discover what one hopes will ultimately be more generalizable methods for the labeling of individual proteins with fluorogenic probes. Although, probe **4** exhibited very slow reactivity towards TTR, it is a non-covalent probe with regard to the timescale of the imaging experiments performed herein. Probe **4** rapidly and efficiently penetrated cell and organelle membranes. Binding-associated activation of probe **3** and probe **4** by TTR seems to be a necessary requirement for TTR conjugation and likely for the modification of other proteins by aryl fluorosulfates, as evidenced by the general lack of reactivity of these probes with more than a few members of the proteome in living cells.

Supplementary Material

Refer to Web version on PubMed Central for supplementary material.

Acknowledgments

We acknowledge NIH grants DK046335 (J.W.K.), DK075295 (J.W.K. and R.L.W.), GM100934 (L.N.), and AI42266 (I.A.W.); the Skaggs Institute for Chemical Biology; The Ellison Medical Foundation (R.L.W. and S.E.E.), Arlene and Arnold Goldstein (S.E.E.), and the Lita Annenberg Hazen Foundation (J.W.K.) for financial support. E.R.G. is supported by the George E. Hewitt Foundation for Medical Research. J.C.G. was supported by the NIH (F32-HL099245) and is currently supported by an American Heart Association fellowship. Y.S.E. is supported by a German Academic Exchange Service (DAAD) postdoctoral fellowship. Portions of this research were carried out at the Stanford Synchrotron Radiation Lightsource, a Directorate of SLAC National Accelerator Laboratory and an Office of Science User Facility operated for the U.S. Department of Energy Office of Science by Stanford University. The SSRL Structural Molecular Biology Program is supported by the DOE Office of Biological and Environmental Research and by the National Institutes of Health, National Institute of General Medical Sciences (including P41GM103393) and the National Center for Research Resources (P41RR001209). We thank Chris Link (University of Colorado), and Cori Bargmann (Rockefeller University), and the *Caenorhabditis* Genetics Center (CGC) for *C. elegans* strains. We are grateful to Colleen Fearns for carefully reading and editing the manuscript.

References

1. Crivat G, Taraska JW. Trends Biotechnol. 2012; 30:8. [PubMed: 21924508]
2. Jing C, Cornish VW. Acc Chem Res. 2011; 44:784. [PubMed: 21879706]
3. Newman RH, Fosbrink M, Zhang J. Chem Rev. 2011; 111:3614. [PubMed: 21456512]
4. Van TNN, Morris MC. Prog Mol Biol Transl. 2013; 113:217.
5. Adams SR, Tsien RY. Nature Protocols. 2008; 3:1527.
6. Soh N. Sensors. 2008; 8:1004.
7. Sun X, Zhang A, Baker B, Sun L, Howard A, Buswell J, Maurel D, Masharina A, Johnsson K, Noren ChJ, Xu MQ, Correa IR. ChemBioChem. 2011; 12:2217. [PubMed: 21793150]
8. Nadler A, Schultz C. Angew Chem Int Ed. 2013; 52:2408.
9. Mizukami S, Hori Y, Kikuchi K. Acc Chem Res. 2013; 47:247. [PubMed: 23927788]
10. Karpenko IA, Kreder R, Valenica Ch, Villa P, Mendre Ch, Mouillac B, ly YM, Hibert M, Bonnet D, Klymchenko AS. ChemBio Chem. 2014; 15
11. Xing B, Khanamiryan A, Rao J. J Am Chem Soc. 2005; 127:4158. [PubMed: 15783183]
12. Zhang H, Fan J, Wang J, Zhang S, Dou B, Peng X. J Am Chem Soc. 2013; 135:11663–11669. [PubMed: 23862760]
13. Lukinavic G, RL, D'Este E, Masharina A, Göttfert F, Ta H, Güther A, Fournier M, Rizzo S, Waldmann H, Blaukopf C, Sommer C, Gerlich DW, Arndt HD, Hell SW, Johnsson K. Nature Methods. 2014; 11:731. [PubMed: 24859753]
14. Han J, Han MS, Tung CH. Mol BioSyst. 2013; 9:3001. [PubMed: 24056749]
15. Choi S, Ong DST, Kelly JW. J Am Chem Soc. 2010; 132:16043. [PubMed: 20964336]
16. Suh EH, Liu Y, Connelly S, Genereux JC, Wilson IA, Kelly JW. J Am Chem Soc. 2013; 135:17869. [PubMed: 24180271]
17. Liu Y, Tan YL, Zhang X, Bhabha G, Ekiert DC, Genereux JC, Cho Y, Kipnis Y, Bjelic S, Baker D, Kelly JW. Proc Natl Acad Sci. 2014; 111:4449. [PubMed: 24591605]
18. Grimm JBH, Lavis LMLD. Prog Mol Biol Transl. 2013; 113
19. Shibata A, Nakano Y, Ito M, Araki M, Zhang J, Yoshida Y, Shuto S, Mannervik B, Mogenstern R, Ito Y, Abe H. Analyst. 2013; 138:7326. [PubMed: 24151635]
20. Baba R, Hori Y, Mizukami S, Kikuchi K. J Am Chem Soc. 2012; 134:14310. [PubMed: 22917182]
21. Smith EL, Bertozzi CR, Beatty KE. ChemBioChem. 2014; 15:1101. [PubMed: 24764280]
22. Sanchini S, Perruccio F, Piizzi G. ChemBioChem. 2014; 15:961. [PubMed: 24719298]
23. Froemming MK, Sames D. J Am Chem Soc. 2007; 128:14518. [PubMed: 17958419]
24. Li L, Ge J, Wu H, Xu QH, Yao SQ. J Am Chem Soc. 2012; 134:12157. [PubMed: 22734946]
25. Grimster NP, Connelly S, Baranczak A, Dong J, Krasnova LB, Sharpless KB, Powers ET, Wilson IA, Kelly JW. J Am Chem Soc. 2013; 135:5656. [PubMed: 23350654]
26. Lang K, Davis L, Wallace S, Mahesh M, Cox DJ, Blackman ML, Fox JM, Chin JW. J Am Chem Soc. 2012; 134:10317. [PubMed: 22694658]
27. Zhuang YD, Chiang PY, Wang CW, Tan KT. Angew Chem Int Ed. 2013; 52:8124.
28. Shieh P, Hangauer MJ, Bertozzi CR. J Am Chem Soc. 2012; 134:17428. [PubMed: 23025473]
29. Kamber DN, Nazarova LA, Liang Y, Lopez SA, Patterson DM, Shih HW, Houk KN, Prescher JA. J Am Chem Soc. 2013; 135:13680. [PubMed: 24000889]
30. Speight LC, Samanta M, Petersson EJ. Aust J Chem. 2014; 67:686.
31. Baranczak A, Connelly S, Liu Y, Choi S, Grimster NP, Powers ET, Wilson IA, Kelly JW. Biopolymers. 2014; 101:484. [PubMed: 24105107]
32. Li X, Gao X, Shi W, Ma H. Chem Rev. 2014; 114:590. [PubMed: 24024656]
33. Loving GS, Sainlos M, Imperiali B. Trends Biotechnol. 2009; 28:73. [PubMed: 19962774]
34. Klymchenko A, Mely Y. Prog Mol Biol Transl. 2013; 113:35.
35. Wiseman RL, Powers ET, Kelly JW. Biochemistry. 2005; 44:16612. [PubMed: 16342952]
36. Schreiber G, Richardson SJ. Comp Biochem Physiol B Biochem Mol Biol. 1997; 116:137. [PubMed: 9159878]

37. Monaco HL, Rizzi M, Coda A. Science. 1995; 268:1039. [PubMed: 7754382]
38. Hammarstrom P, Wiseman RL, Powers ET, Kelly JW. Science. 2003; 299:713. [PubMed: 12560553]
39. Wojtczak A, Cody V, Luft JR, Pangborn W. Acta Crystallogr D Biol Crystallogr. 1996; 52:758. [PubMed: 15299640]
40. Rappley I, Monteiro C, Novais M, Baranczak A, Solis G, Wiseman RL, Helmke S, Maurer MS, Coelho T, Powers ET, Kelly JW. Biochemistry. 2014; 53:1993. [PubMed: 24661308]
41. Berk JL, Suhr OB, Obici L, Sekijima Y, Zeldenrust SR, Yamashita T, Hennegan MA, Gorevic PD, Litchy WJ, Wiseman JF, Nordh E, Corato M, Lozza A, Cortese A, Robinson-Papp J, Colton T, Rybin DV, Bisbee AB, Ando Y, Ikeda S, Seldin DC, Merlini G, Skinner M, Kelly JW, Dyck PJ. J Am Med Assoc. 2013; 310:2658.
42. Bulawa CE, Connelly S, DeVit M, Wang L, Weigel C, Fleming JA, Packman J, Powers ET, Wiseman RL, Foss TR, Wilson IA, Kelly JW, Labaudiniere R. Proc Natl Acad Sci U S A. 2012; 109:9629. [PubMed: 22645360]
43. Coelho T, Maia LF, Martins DSA, Waddington CM, Plante-Bordeneuve V, Lozeron P, Suhr OB, Campistol JM, Conceicao IM, Schmidt HHJ, Trigo P, Kelly JW, Labaudiniere R, Chan J, Packman J, Wilson A, Grogan DR, Imventarza OC, Wainberg PJ, Berra LM, Maultasch H, Gold J, Bardera JCP, Zibert A. Neurology. 2012; 79:785. [PubMed: 22843282]
44. Coelho T, Maia LF, da Silva AM, Cruz MW, Plante-Bordeneuve V, Suhr OB, Conceicao I, Schmidt HH, Trigo P, Kelly JW, Labaudiniere R, Chan J, Packman J, Grogan DR. J Neurol. 2013; 260:2802. [PubMed: 23974642]
45. Dong J, Krasnova L, Finn MG, Sharpless KB. Angew Chem Int Ed. 2014; 53:2.
46. Otwinowski Z, Minor W. Methods Enzymol. 1997; 276:307.
47. Emsley P, Cowtan K. Acta Crystallogr D Biol Crystallogr. 2004; 60:2126. [PubMed: 15572765]
48. Murshudov GN, Skubák P, Lebedev AA, Pannu NS, Steiner RA, Nicholls RA, Winn MD, Long F, Vagin AA. Acta Crystallogr D Biol Crystallogr. 2011; 67:355. [PubMed: 21460454]
49. Lebedev AA, Young P, Isupov MN, Moroz OV, Vagin AA, Murshudov GN. Acta Crystallogr D Biol Crystallogr. 2012; 68:431. [PubMed: 22505263]
50. Lovell SC, Davis IW, Arendall WB 3rd, de Bakker PI, Word JM, Prisant MG, Richardson JS, Richardson DC. Proteins. 2003; 50:437. [PubMed: 12557186]
51. Vriend G. J Mol Graph. 1990; 8:52. [PubMed: 2268628]
52. Terwilliger TC. Acta Crystallogr D Biol Crystallogr. 2003; 59:38. [PubMed: 12499537]
53. Brenner S. Genetics. 1974; 77:71. [PubMed: 4366476]
54. Mello C, Fire A. Meth in Cell Biol. 1995; 48:451.
55. Solis GM, Petrascheck M. J Visual Exp. 2011; 49:2496. [PubMed: 21445049]
56. Lange W, Muller E. Chem Ber. 1930; 63:2653.
57. Stevens TE. J Org Chem. 1968; 33:2664.
58. Roth GP, Fuller CE. J Org Chem. 1991; 56:3493.
59. Hedayatullah M, Hugueny JC, Guy A. J Het Chem. 1984; 21:1385.
60. Roth GI, Thomas JA. Tetrahedron Lett. 1992; 33:1959.
61. Hedayatullah M, Guy A, Denivelle L. C R Acad Sc Paris. 1974; 278:57.
62. Hedayatullah M, Guy A, Denivelle L. Phosphorus, sulfur and silicon and related elements. 1980; 8:125.
63. Ishii, A.; Ishimaru, T.; Yamazaki, T.; Yasumoto, M. WO 2013002040. 2013.
64. Choi S, Connelly S, Reixach N, Wilson IA, Kelly JW. Nat Chem Bio. 2010; 6:133. [PubMed: 20081815]
65. Murphy MP. Curr Opin Investig Drugs. 2009; 10:1022.
66. Shapira AHV. The Lancet. 2012; 379:1825.
67. Yousif LF, Stewart KM, Kelley SO. ChemBioChem. 2009; 10:1939. [PubMed: 19637148]
68. Smith RAJ, Hartley RC, Murphy MP. Antioxidants & Redox Signaling. 2011; 15:3021. [PubMed: 21395490]

69. Rainbolt TK, Atanassova N, Genereux JC, Wiseman RL. Cell Metabolism. 2013; 18:908. [PubMed: 24315374]
70. Link CD. Proc Natl Acad Sci. 1995; 92:9368. [PubMed: 7568134]
71. Petrascheck M, Ye X, Buck LB. Nature. 2007; 450:553. [PubMed: 18033297]
72. Fang-Yen C, Gabel ChV, Samuel ADT, Bargmann CI, Avery L. Methods Cell Biol. 2012; 107:177. [PubMed: 22226524]
73. Fares H, Greenwald I. Genetics. 2001; 159:133. [PubMed: 11560892]
74. Maniar TA, Kaplan M, Wang GJ, Shen K, Wei L, Shaw JE, Koushika SP, Bargmann CI. Nat Neurosci. 2012; 15:48. [PubMed: 22101643]
75. Sekijima Y, Wiseman RL, Matteson J, Hammarström P, Miller SR, Sawkar AR, Balch WE, Kelly JW. Cell. 2005; 21:73. [PubMed: 15820680]
76. Lakowicz JR, Gryczynski I, Malak H, Gryczynski Z. J Phys Chem. 1996; 100:19406.
77. Bolton O, Kim J. J Mater Chem. 2007; 17:1981.
78. Reddy MA, Mallesham G, Thomas A, Srinivas K, Rao VJ, Bhanuprakash K, Giribabu L, Grover R, Kumar A, Kamalasanan MN, Srivastava R. Synth Met. 2011; 161:869.
79. Hughes G, Kreher D, Wang Ch, Batsanov AS, Bryce MR. Org Biomol Chem. 2004; 2:3363. [PubMed: 15534714]
80. Oliveira CS, Lira BF, Barbosa-Filho JM, Fernandez Lorenzo JG, Filgueiras de Athayde-Filho P. Molecules. 2012; 17:10192. [PubMed: 22926303]
81. Kim YK, Lee JK, Lee JS, Yoon CN, Chang YT. Mol Biosyst. 2011; 7:2375. [PubMed: 21660325]
82. Gales L, Saraiva MJ, Damas AM. Biochim Biophys Acta. 2007; 1774:59. [PubMed: 17175208]
83. Lima LM, Silva V, de A, de Palmieri LC, Oliveira MC, Foguel D, Polikarpov I. Bioorg Med Chem. 2010; 18:100. [PubMed: 19954984]
84. Johnson SM, Connelly S, Wilson IA, Kelly JW. J Med Chem. 2009; 52:1115. [PubMed: 19191553]
85. Suydam IT, Snow CD, Pande VS, Boxer SG. Science. 2006; 313:200. [PubMed: 16840693]
86. Sirin GS, Zhou Y, Lior-Hoffmann L, Wang S, Zhang Y. J Phys Chem. 2012; 116:12199.
87. Bojarov P, Denehy E, Walker I, Loft K, De Souza DP, Woo LWL, Potter BVL, McConville MJ, Williams SJ. ChemBioChem. 2008; 9:613. [PubMed: 18288656]
88. Vane JR, Botting RM. Thrombosis Res. 2003; 110:255.
89. Colon W, Kelly JW. Biochemistry. 1992; 31:8654. [PubMed: 1390650]
90. Lai Z, Colon W, Kelly JW. Biochemistry. 1996; 35:6470. [PubMed: 8639594]
91. Connelly S, Choi S, Johnson SM, Kelly JW, Wilson IA. Curr Op Struct Biol. 2010; 20:54.
92. Lavis LD, Raines RT. ACS Chem Biol. 2014; 9:855. [PubMed: 24579725]
93. Kobayashi H, Ogawa M, Alford R, Choyke PL, Urano Y. Chem Rev. 2010; 110:2620. [PubMed: 20000749]

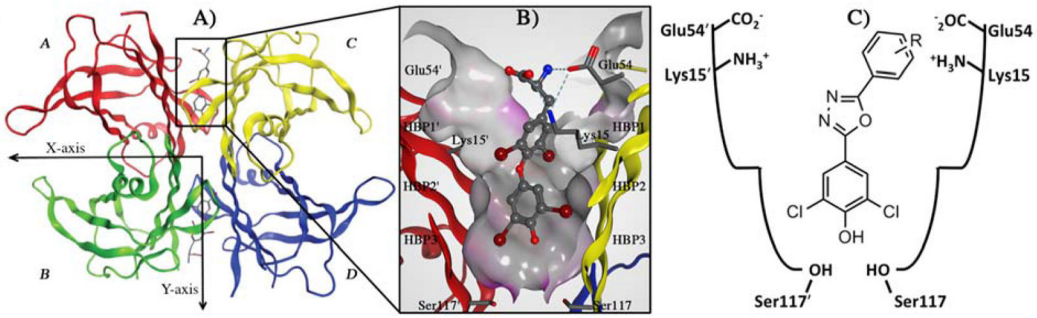

Figure 1.

Structure of homo-tetrameric TTR^{WT} and its T_4-binding pockets. (A) Crystal structure of TTR^{WT} in complex with two thyroxine (T_4) molecules (PDB 2ROX)[43]. (B) Close-up view of one of the two identical T_4-binding sites showing a ribbon diagram depicted tetramer (colored by chain) with a "Connolly" molecular surface applied to residues within 8 Å of T_4 (hydrophobic = gray, polar = purple). The innermost halogen binding pockets (HBPs) 3 and 3′ are composed of the methyl and methylene groups of Ser117/117′, Thr119/119′, and Leu110/110′. HBPs 2 and 2′ are formed by the side chains of Leu110/110′, Ala109/109′, Lys15/15′, and Leu17/17′. The outermost HBPs 1 and 1′ are lined by the methyl and methylene groups of Lys15/15′, Ala108/108′, and Thr106/106′. These figures were generated using the program MOE (2011.10). (C) Schematic representation of the T_4-binding pocket with the amino acids that are being targeted in the design and optimization of fluorogenic probes. R = SO_2F or OSO_2F.

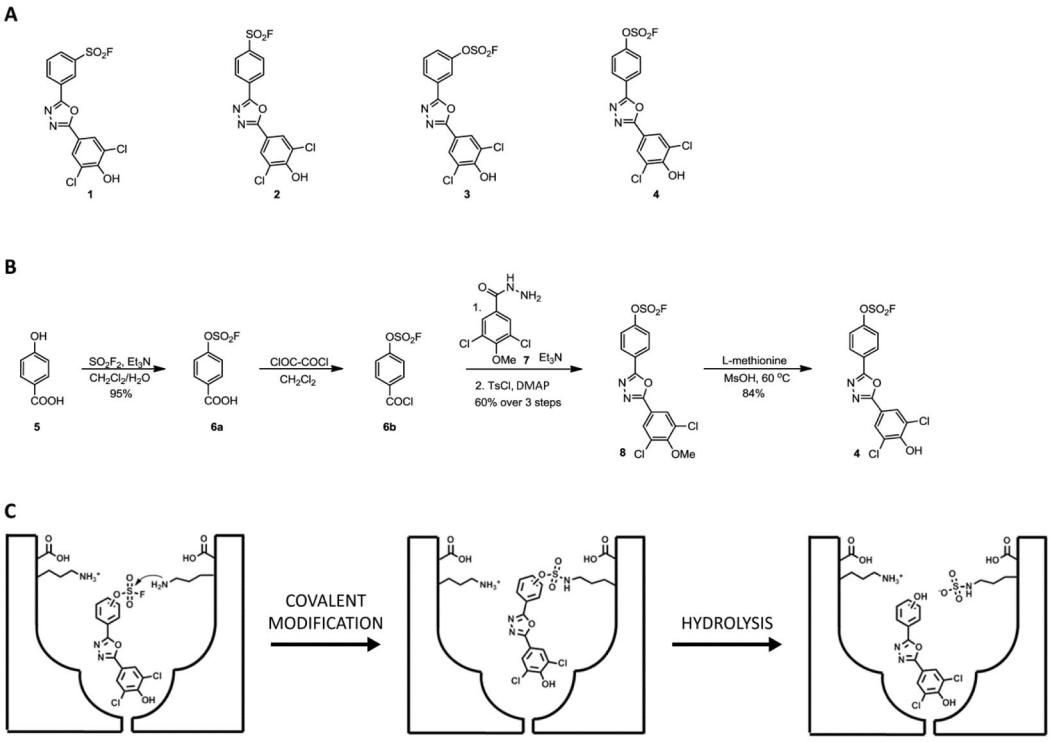

Figure 2.

(A) Chemical structures of probes **1** – **4**. (B) Synthesis of fluorosulfate **4**. (C) An illustration of the fate of some fluorosulfates such as probe **3** in the T_4-binding pocket. TTR and probe **3** initially form a non-covalent complex. Then reaction of the fluorosulfate group with the Lys15 residue leads to the formation of a TTR-ligand conjugate which subsequently undergoes hydrolysis to produce sulfamated TTR and the non-covalently bound phenol hydrolysis product, a reaction that may be catalyzed by TTR.

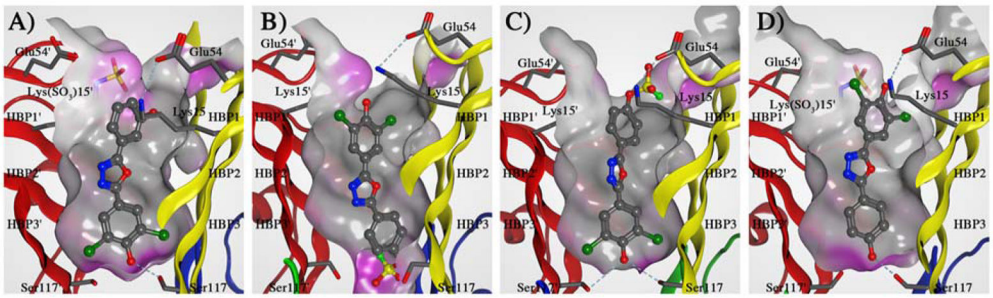

Figure 3.

Crystal structures of homo-tetrameric TTR^{WT} after binding and/or binding and reaction with probe **3** or probe **4**. (A) The product after probe **3** reacted with TTR^{WT}. (B) Probe **4** bound in the 'forward' orientation. (C) Probe **4** bound in the 'reverse' orientation. (D) The product of the very slow reaction between probe **4** and TTR^{WT}. Each panel represents a close-up view of one of the two identical T_4-binding sites as a ribbon diagram depicted tetramer colored by chain. A "Connolly" molecular surface was applied to residues within 8 Å of ligand in the T_4-binding pocket; hydrophobic (grey), polar (purple). The innermost HBPs 3 and 3′ are composed of the methyl and methylene groups of Ser117/117′, Thr119/119′, and Leu110/110′. HBPs 2 and 2′ are formed by the side chains of Leu110/110′, Ala109/109′, Lys15/15′, and Leu17/17′. The outermost HBPs 1 and 1′ are lined by the methyl and methylene groups of Lys15/15′, Ala108/108′, and Thr106/106′. Hydrogen bonds are shown in light blue dashed lines. This figure was generated using the program MOE (2011.10), Chemical Computing Group, Montreal, Canada.

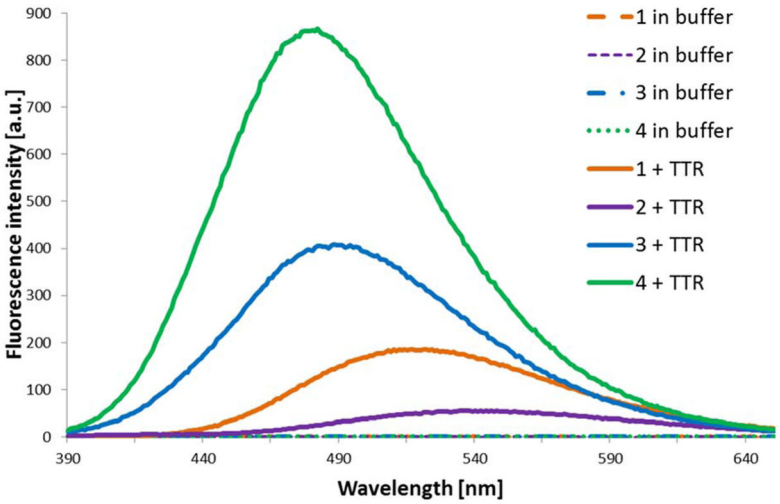

Figure 4.

Fluorescence emission spectra of probes **1**, **2**, **3**, and **4** (7.2 μM) in buffer and bound to TTR^{WT} (3.6 μM) after 1 h incubation at 37 °C. Probe **1** forms a conjugate with TTR^{WT} with 42% yield (max. modification is 50%) after a 1 h incubation period. Probe **2** forms a conjugate with TTR^{WT} with 21% yield after a 1 h incubation period. Effectively, probe **3** and probe **4** do not react with TTR^{WT} within 1 h.

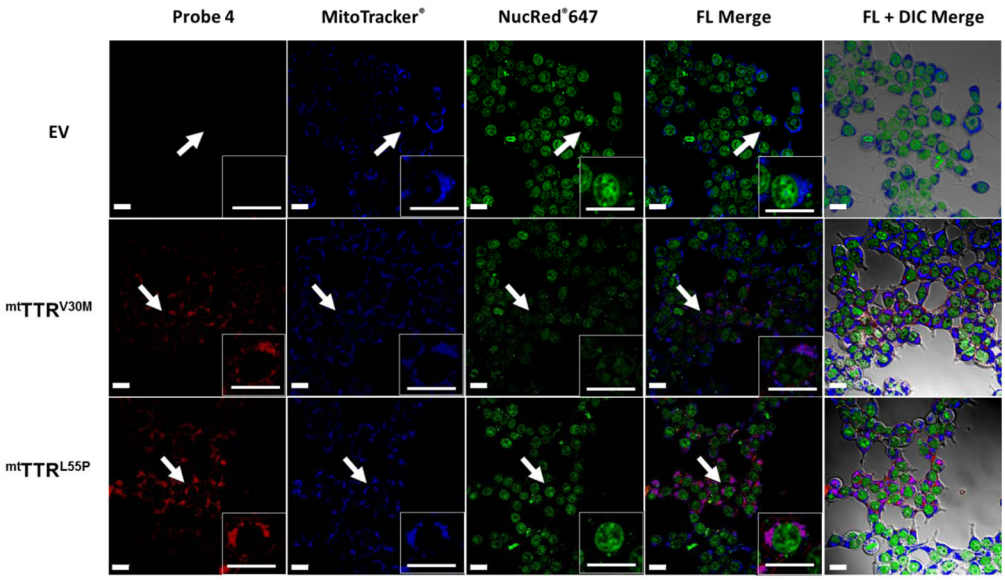

Figure 5.

Confocal fluorescence microscopy images of living HEK293T cells transfected with an empty vector (EV; pcDNA3.1(+)) or $^{mt}TTR^{V30M}$ or $^{mt}TTR^{L55P}$ constructs, and treated with probe **4** (20 μM) for 20 min, followed by a 30-min incubation/diffusion period in probe-free media prior to imaging. Fluorescent image labels: probe **4** = red, mitochondrial stain - MitoTracker® Orange = blue, nucleus stain - NucRed® = green, FL Merge = fluorescence signal overlap, FL + DIC Merge = fluorescence and bright-field overlap. Scale bar = 20 μm. Arrows indicate the cells shown at higher magnification in the insets. Identical microscope settings were used for acquisition of TTR-transfected and EV-transfected cell images.

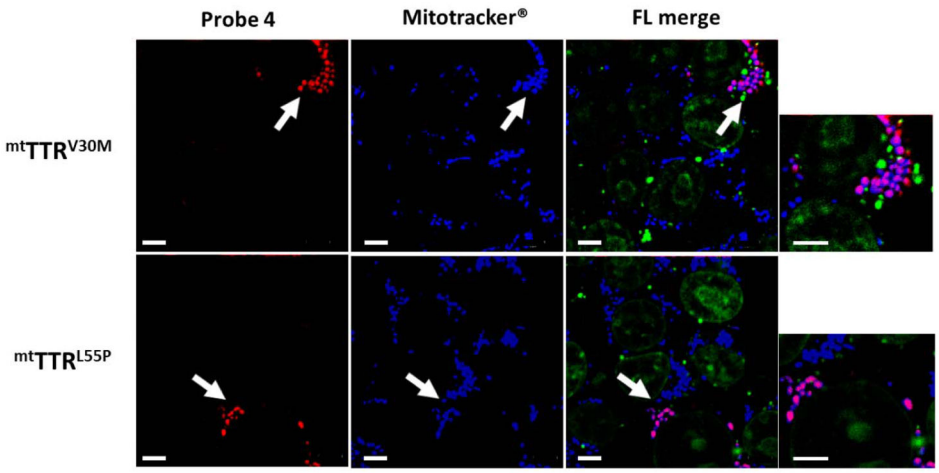

Figure 6.

Confocal fluorescence microscopy images of living HEK293T cells transfected with $^{mt}TTR^{V30M}$ or $^{mt}TTR^{L55P}$ constructs, and treated with probe **4** (5 μM) for 30 sec, followed by a 10 min incubation/diffusion period in probe-free media prior to imaging. Fluorescent images labels: probe **4** = red, mitochondrial stain - MitoTracker® Orange = blue, nucleus stain - NucRed® = green, FL Merge = fluorescence signal overlap. Scale bar = 5 μm. Arrows indicate the cells shown at higher magnification (far right panels).

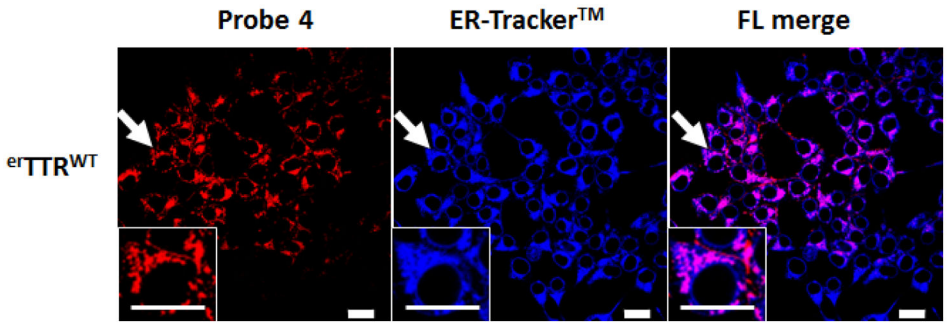

Figure 7.

Confocal fluorescence microscopy images of living HEK293T cells transfected with $^{er}TTR^{WT}$ construct and treated with probe **4** (5 μM) for 30 sec, followed by a 15 min incubation/diffusion period in probe-free media. Fluorescent image labels: probe **4** = red, ER stain - ER-Tracker™ Green = blue, FL Merge = fluorescence signal overlap. Scale bar = 20 μm. Arrows indicate the cells shown at higher magnification in the insets.

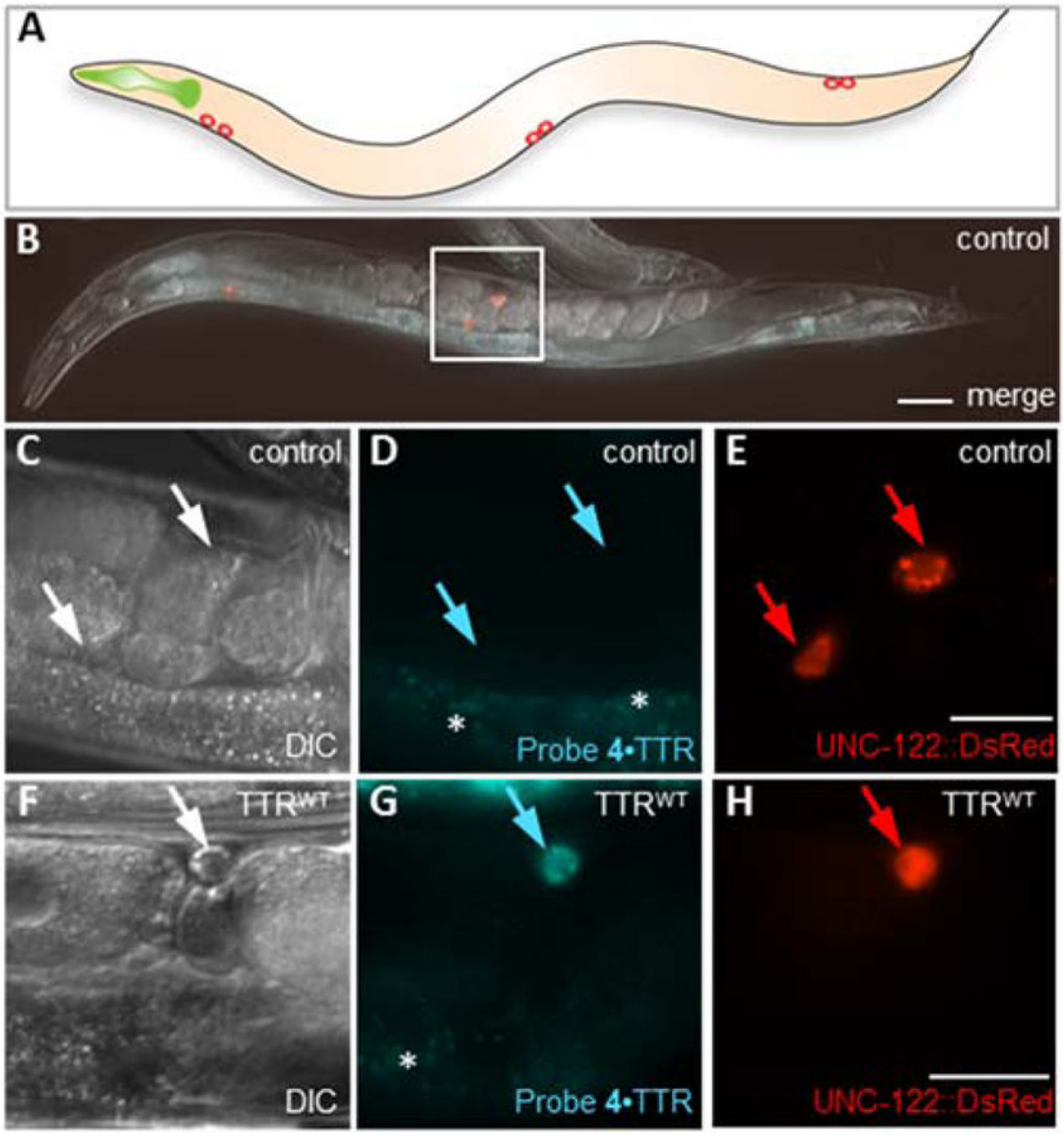

Figure 8.

In vivo labeling of TTR^{WT} in coelomocytes of *C. elegans* with probe **4.** (A) Schematic of a *C. elegans* worm showing the position of the six coelomocytes in red. The pharynx is shown in green. (B) Merged Nomarski differential interference contrast (DIC) photomicrograph and fluorescent images of a probe **4**-treated control *(rol-6)* day 2 adult worm. All fluorescent images have the following labels: red = UNC-122::DsRed-labeled coelomocytes (3 are seen in this focal plane); cyan = probe **4**. Scale bar = 50 μm. (C–E) Enlargement images of boxed region of the same worm shown in B. Arrows point to two coelomocytes in the focal plane. Scale bar = 25 μm. (F–H) Enlargement images of a day 2 old worm expressing TTR^{WT} treated with probe **4.** Arrow points to a coelomocyte in the focal plane. Scale bar = 25 μm. Asterisks denote unspecific gut autofluorescence, observed in untreated *C. elegans*, as well

as in *C. elegans* treated with probe **4**; see Figure S20. Identical microscope settings were used for acquisition of control and TTR transgenic worm images.